J. Fluid. Mech. (1989), *vol.* 206, *pp.* 497–515
Printed in Great Britain

The effects of temperature-dependent viscosity and the instabilities in convection rolls of a layer of fluid-saturated porous medium

By A. C. OR†
Division of Applied Sciences, Harvard University, Cambridge, MA 02138, USA

(Received 14 March 1988)

Convection of two-dimensional rolls in an infinite horizontal layer of fluid-saturated porous medium heated from below is studied numerically. Several important finite-amplitude states are isolated, and their bifurcation properties are shown. Effects of the temperature-dependent viscosity are included. The stability of these states is investigated with respect to the class of disturbances that have a $\frac{1}{2}\pi$ phase shift relative to the basic state. In particular, the oscillatory mechanism and the mean-flow generating mechanism through the variable viscosity are discussed.

1. Introduction

Thermal convection in a fluid-saturated porous medium has been a subject of fundamental interest in the stability of fluid flows. The reasons are: (i) It is dynamically simpler than other convective systems since the nonlinearity only appears in the advection of the temperature field. This feature is similar to that in Rayleigh–Bénard convection at infinite Prandtl number. However, unlike the latter system, convection in the porous probelm is governed by a lower-order differential equation of motion, since the boundary condition only restricts the normal velocity component. (ii) The two-dimensional rolls in a porous medium have the same governing equations as the ordinary convection rolls in a Hele–Shaw apparatus (Saffman & Taylor 1958). These properties make the results of the two-dimensional porous-convection problem of physical significance, even in the region where the three-dimensional motions in fact predominate. The numerical two-dimensional studies in the porous rolls can provide direct comparisons with the Hele–Shaw experiments. (iii) The porous rolls have been found to exhibit two-dimensional oscillations (Combarnous & Le Fur 1969; Horne & O'Sullivan 1974, 1978; Schubert & Straus 1982; Kimura, Schubert & Straus 1986; Aidun & Steen 1987; and Steen & Aidun 1988). The two-dimensional problem provides a relatively simple example in studies of the transition to turbulence in pattern forming systems. In contrast, the analogous oscillatory instabilities have not been observed in the two-dimensional numerical solutions of ordinary convection, even for a Rayleigh number up to as high as 25 times above the critical onset.

In all the porous-convection studies cited above, the investigators focused on a unicellular pattern in a square cross-section. The numerical analyses are two-dimensional. Since the sidewalls are insulated and no derivatives of the velocity field are restricted, the unicellular patter satisfies the conditions required for periodically

† Present address: Hughes Aircraft Company, S & CG, S41, B320, P.O. Box 92919, CA 90009, USA.

continuing the pattern to an infinite extent. For the basic finite-amplitude solution, the unicellular problem in a square section is identical to that in an infinite layer with the wavenumber prescribed at the critical onset value. Restricted by the sidewalls, the instabilities, however, can only correspond to a restricted class of in-phase disturbances. For a infinite-periodic system, the instabilities can have the freedom of a $\frac{1}{2}\pi$ phase shift relative to the basic state.

In this paper, we consider the porous-medium convection in an infinite horizontal layer of fluid. The main features of this study are: (i) the temperature dependent viscosity is included; (ii) several finite-amplitude equilibria, other than the basic solutions, are identified and their bifurcation structures are studied; (iii) the stability analysis of the steady solution with respect to the $\frac{1}{2}\pi$ phase-shifted disturbances.

Of particular importance are the class of oscillatory instabilities and the instabilities with a non-vanishing mean vorticity component. The latter instabilities show the tendency of driving a mean flow through the viscosity gradient. The oscillatory instabilities appear to be an interesting feature for the lower-order porous system. This class of instabilities has received much emphasis. Although the sequence of transitions has been fairly accurately determined as a function of the control parameter, the driving mechanism of the phenomenon remains unclear. This problem will be treated through a truncated model here. Some important qualitative aspects of the mechanism can be explored. These aspects are rather difficult to reveal from the full numerical simulations.

From a somewhat different perspective, the mean-flow generation mechanism is of interest in the geophysical context. The possibility of a mean-flow driving mechanism through the temperature-dependent viscosity was suggested by Busse (1983). The search for a disturbance eigenmode associated with a mean component of vorticity that exhibits an exponential growth poses an interesting problem. For this reason we choose to examine the class of instabilities with a $\frac{1}{2}\pi$ phase shift relative to the basic solutions. The problem has been partly motivated by the observation of mean drift in the continents (Hager & O'Connell 1981). The data suggest, under the hypothesis of a convective mantle, that the mean flow requires a driving mechanism other than the Reynolds stresses. This is because the Earth's mantle resembles an infinite-Prandtl-number fluid, and thus has vanishing Reynolds stresses.

2. Formulation of the mathematical problem

The configuration to be considered is an infinitely extended horizontal porous layer filled with fluid and heated from below. The layer has a thickness d and is bounded by two parallel plates which are kept at fixed temperatures. Density and viscosity of the fluid exhibit a linear dependence on the temperature,

$$\rho = \rho_0(1-\gamma(T-T_0)), \tag{2.1a}$$

$$\mu = \mu_0(1-\beta^*(T-T_0)), \tag{2.1b}$$

where T_0 refers to the median of the temperatures T_1, T_2 imposed at the boundaries. While ρ varies little throughout the porous layer in accordance with the Boussinesq approximation, the viscosity may vary by an order of magnitude or more. Using $d, d^2/\kappa$, and the positive temperature difference between the lower and upper plate,

T_2-T_1, as scales for length, time and temperature, respectively, we obtain the dimensionless Darcy–Boussinesq equations for convection in a porous layer

$$-(\beta(z-\theta)+1)\,\boldsymbol{u}+Rk\theta-\nabla\pi=0, \tag{2.2a}$$

$$\nabla\cdot\boldsymbol{u}=0, \tag{2.2b}$$

$$\nabla^2\theta+\boldsymbol{u}\cdot\boldsymbol{k}=\partial_t\theta+\boldsymbol{u}\cdot\nabla\theta, \tag{2.2c}$$

where $\boldsymbol{u}$ is the velocity averaged over the microscale of the porous medium and θ describes the deviation of the temperature from the static distribution. The unit vector in the direction opposite to gravity is denoted by $\boldsymbol{k}$, and the dimensionless parameters β, R are defined by

$$R=\frac{\gamma g(T_2-T_1)K\rho d}{\mu_0\kappa}, \tag{2.3a}$$

$$\beta=\beta^*(T_2-T_1). \tag{2.3b}$$

The thermal diffusivity κ is defined as the thermal conductivity of the fluid–solid mixture divided by the specific heat and the density of the fluid. K is the Darcy permeability coefficient and g is the acceleration due to gravity.

We shall use a Cartesian system of coordinates with the z-coordinate in the direction of $\boldsymbol{k}$. Since the analysis will be limited to two-dimensional flow, it is convenient to introduce the stream function ψ,

$$\boldsymbol{u}=\nabla\times j\psi(x,z,t),$$

where $\boldsymbol{j}$ is the unit vector in the y-direction. After taking the y-component of the curl of (2.2a), the basic equations (2.2) can be replaced by

$$(\beta(z-\theta)+1)\,\nabla^2\psi+\beta\partial_z(z-\theta)\,\partial_z\psi-\beta\partial_x\theta\partial_x\psi-R\partial_x\theta=0, \tag{2.4a}$$

$$\nabla^2\theta+\partial_x\psi+\partial_z\psi\partial_x\theta-\partial_x\psi\partial_z\theta=\partial_t\theta, \tag{2.4b}$$

where ∂_z indicates the partial derivative with respect to z.

Steady solutions of (2.4) can be obtained by expanding ψ, θ in series of functions satisfying the boundary conitions

$$\psi=\theta=0 \quad \text{at} \quad z=\tfrac{1}{2},\ -\tfrac{1}{2}. \tag{2.5}$$

Trigonometric functions are the obvious choice for both the x- and the z-directions. The symmetry of the problem permits solutions that have a symmetric temperature distribution with respect to the x-direction,

$$\theta=\sum_{l,n}^{\infty}B_{ln}\cos l\alpha x\sin n\pi(z-\tfrac{1}{2}), \tag{2.6a}$$

$$\psi=\sum_{l,n}^{\infty}A_{ln}\sin l\alpha x\sin n\pi(z-\tfrac{1}{2}). \tag{2.6b}$$

After inserting (2.6) into (2.4), multiplying (2.4a, b) by $4\sin k\alpha x\sin m\pi(z-\frac{1}{2})$ and $4\cos k\alpha x\sin m\pi(z-\frac{1}{2})$, respectively, and averaging the result over the fluid layer, the following system of algebraic equations is obtained:

$$D_{kmln}A_{ln}-Rl\alpha\delta_{k,l}\delta_{n,m}B_{ln}-\tfrac{1}{2}\beta[kl\alpha^2(\delta_{k,l+p}+\delta_{k,l-p}+\delta_{k,p-l})\,e_{nmr}+nm\pi^2(\delta_{k,l+p}+\delta_{k,l-p}-\delta_{k,p-l})\,\hat{e}_{nmr}]A_{ln}B_{pr}=0, \tag{2.7a}$$

$$(l^2\alpha^2+n^2\pi^2)(1+d(k))\,\delta_{k,l}\delta_{n,m}B_{ln}-l\alpha\delta_{k,l}\delta_{n,m}A_{ln}$$
$$+\tfrac{1}{4}\alpha\pi[pn(\delta_{p,l+k}+\delta_{p,l-k}-\delta_{p,k-l})(\delta_{m,r+n}-\delta_{m,n-r}+\delta_{m,r-n})$$
$$+lr(\delta_{k,l+p}+\delta_{k,l-p}+\delta_{k,p-l})(\delta_{m,r+n}+\delta_{m,n-r}-\delta_{m,r-n})]A_{ln}B_{pr}=0, \quad (2.7b)$$

where $\delta_{i,j}$ is the Kronecker symbol and the convention of summation over subscripts occurring twice in any term is assumed. The following definitions have been used:

$$D_{kmln}=kl\alpha^2\delta_{k,l}(\delta_{n,m}+\beta d_{nm})+nm\pi^2\delta_{k,l}(\delta_{n,m}+\beta\hat{d}_{nm}), \quad (2.8a)$$

$$d_{nm}=\begin{cases}2((m-n)^{-2}-(n+m)^{-2})/\pi^2 & \text{for odd } m+n\\ 0 & \text{for even } m+n,\end{cases} \quad (2.8b)$$

$$\hat{d}_{nm}=\begin{cases}2((m-n)^{-2}+(n+m)^{-2})/\pi^2 & \text{for odd } m+n\\ 0 & \text{for even } m+n,\end{cases} \quad (2.8c)$$

$$e_{nmr}=\begin{cases}((m+n+r)^{-1}+(m-n-r)^{-1}-(m+n-r)^{-1}-(m-n+r)^{-1})/\pi & \text{odd } m+n+r\\ 0 & \text{even } m+n+r,\end{cases} \quad (2.8d)$$

$$\hat{e}_{nmr}=\begin{cases}(-(m+n+r)^{-1}+(m-n-r)^{-1}+(m+n-r)^{-1}-(m-n+r)^{-1})/\pi & \text{odd } m+n+r\\ 0 & \text{even } m+n+r.\end{cases} \quad (2.8e)$$

$$d(k)=\begin{cases}0 & \text{for } k\neq 0\\ 1 & \text{for } k=0.\end{cases} \quad (2.8f)$$

Equation (2.7) can be solved by a Newton–Raphson iteration method once a truncation of the infinite system is introduced. As in earlier works on nonlinear convection (see, for example, Busse 1967) the truncation will be accomplished by neglecting all coefficients and equations with subscripts satisfying

$$k+l>NT. \quad (2.9)$$

The truncation parameter NT is chosen such that properties like the convective heat transport change by a few percent at most when NT is replaced by $NT+2$.

The stability of the two-dimensional solutions for the convection rolls will be considered with respect to a restricted class of disturbances. The problem of stability with respect to more general classes of disturbances has been considered by Straus & Schubert (1979) and Schubert & Straus (1979) in the case of constant viscosity. We shall restrict attention to a particular class of disturbances. This class of disturbance is associated with the mechanism of mean-flow generation in a porous medium owing to temperature-dependent viscosity.

The equations for infinitesimal two-dimensional disturbances $\tilde{\psi}$, $\tilde{\theta}$ of the steady solutions ψ, θ can be written in the form

$$(\beta(z-\theta)+1)\nabla^2\tilde{\psi}-\beta[\tilde{\theta}\nabla^2\psi-\partial_z(z-\theta)\partial_z\tilde{\psi}+\partial_z\tilde{\theta}\partial_z\psi+\partial_x\theta\partial_x\tilde{\psi}+\partial_x\tilde{\theta}\partial_x\psi]-R\partial_x\tilde{\theta}=0, \quad (2.10a)$$

$$\nabla^2\tilde{\theta}+\partial_x\tilde{\psi}+\partial_z\psi\partial_x\tilde{\theta}+\partial_z\tilde{\psi}\partial_x\theta-\partial_x\psi\partial_z\tilde{\theta}-\partial_x\tilde{\psi}\partial_z\theta=\sigma\tilde{\theta}, \quad (2.10b)$$

where a time dependence of the form $\exp(\sigma t)$ has been assumed for the disturbances. Equations (2.10) admit, among others, solutions $\tilde{\theta}$ which are symmetric or

antisymmetric in x. Here we focus the attention on the latter kind and use the representation

$$\tilde{\theta} = \hat{\theta}\exp\sigma t = \sum_{l,n}^{\infty} \tilde{B}_{ln}\sin l\alpha x \sin n\pi(z-\tfrac{1}{2})\exp\alpha\sigma t, \tag{2.11a}$$

$$\tilde{\psi} = (\hat{\psi} - \int U(z)\,\mathrm{d}z)\exp\sigma t = \left[\sum_{l,n}^{\infty} \tilde{A}_{ln}\cos l\alpha x \sin n\pi(z-\tfrac{1}{2}) - \int U(z)\,\mathrm{d}z\right]\exp\sigma t. \tag{2.11b}$$

In contrast to the steady solution, the disturbance may involve a mean flow which has been separated in (2.11b) because the boundary conditions for $\tilde{\psi}$ at $z = -\frac{1}{2}, \frac{1}{2}$ apply only for the fluctuating component. By returning to the original equations (2.2) a simple expression can be obtained for the mean flow in the x-direction,

$$U(z) = -\beta(\overline{\hat{\theta}\partial_z\hat{\psi}} + \overline{\theta\partial_z\hat{\psi}})\,(1+\beta(z-\bar{\theta}))^{-1}, \tag{2.12}$$

where the bar indicates the horizontal average. The equations for the coefficients $\tilde{A}_{pn}, \tilde{B}_{pn}$ are derived from (2.10) in the same way as the corresponding equation in the steady case,

$$\begin{aligned} &D_{kmln}\tilde{A}_{ln} + Rl\alpha\delta_{k,l}\delta_{n,m}\tilde{B}_{ln} - \tfrac{1}{2}\beta\tilde{A}_{ln}B_{pr}[kl\alpha^2(\delta_{k,l+p}+\delta_{k,l-p}-\delta_{k,p-l})\,e_{nmr} \\ &\quad + nm\pi^2(\delta_{k,l+p}+\delta_{k,l-p}+\delta_{k,p-l})\,\hat{e}_{nmr}] - \tfrac{1}{2}\beta A_{ln}\tilde{B}_{pr}[kl\alpha^2(\delta_{l,k+p}-\delta_{l,p-k}-\delta_{l,k-p})\,e_{nmr} \\ &\quad + nm\pi^2(\delta_{p,l+k}+\delta_{p,l-k}-\delta_{p,k-l})\,\hat{e}_{nmr}] - \tfrac{1}{4}\beta^2 mr\pi^2(A_{pr}\tilde{B}_{pn}+B_{pn}\tilde{A}_{pr})\,(\delta_{s,n+r}+\delta_{s,n-r} \\ &\qquad -\delta_{s,r-n})\,\hat{W}_{smq}B_{kq} = 0, \end{aligned} \tag{2.13a}$$

where $$\hat{W}_{smq} = \int_{-\frac{1}{2}}^{\frac{1}{2}} \sin s\pi(z-\tfrac{1}{2})\cos m\pi(z-\tfrac{1}{2})\sin q\pi(z-\tfrac{1}{2})\,(1+\beta(z-\bar{\theta}))^{-1}\,\mathrm{d}z$$

and $$\bar{\theta} = \sum_{n}^{\infty} B_{on}\sin n\pi(z-\tfrac{1}{2});$$

$$\begin{aligned} &(l^2\alpha^2+n^2\pi^2+\sigma)\,(1+d(k))\,\delta_{k,l}\delta_{n,m}\tilde{B}_{ln} + l\alpha\delta_{k,l}\delta_{n,m}\tilde{A}_{ln} \\ &\quad + \tfrac{1}{4}\alpha\pi[pn(\delta_{k,l+p}+\delta_{k,p-l}-\delta_{k,l-p})\,(\delta_{m,r+n}-\delta_{m,n-r}+\delta_{m,r-n}) \\ &\quad + lr(-\delta_{k,l+p}-\delta_{k,l-p}+\delta_{k,p-l}) \\ &\qquad \times(\delta_{m,r+n}+\delta_{m,n-r}-\delta_{m,r-n})]\tilde{A}_{ln}B_{pr} + \tfrac{1}{4}\alpha\pi[pn(-\delta_{k,l+p}-\delta_{k,l-p}+\delta_{k,p-l}) \\ &\qquad \times(\delta_{m,r+n}-\delta_{m,n-r}+\delta_{m,r-n}) + lr(\delta_{k,l+p}-\delta_{k,l-p}+\delta_{k,p-l}) \\ &\qquad \times(\delta_{m,r+n}+\delta_{m,n-r}-\delta_{m,r-n})]A_{ln}\tilde{B}_{pr} \\ &\qquad + \tfrac{1}{2}\beta kr\alpha\pi(B_{pn}\tilde{A}_{pr}+\tilde{B}_{pn}A_{pr})\,(\delta_{s,n+r}+\delta_{s,n-r}-\delta_{s,r-n})\,W_{smq}B_{kq} = 0, \end{aligned} \tag{2.13b}$$

where the definition

$$W_{smq} = \int_{-\frac{1}{2}}^{\frac{1}{2}} \sin s\pi(z-\tfrac{1}{2})\sin m\pi(z-\tfrac{1}{2})\sin q\pi(z-\tfrac{1}{2})\,(1+\beta(z-\bar{\theta}))^{-1}\,\mathrm{d}z$$

has been used.

3. Finite-amplitude steady states

For $R > R_c$, there exists a pair of α-values on the neutral curve. It is thus not surprising that the bimodal interaction can occur. Such interaction can give rise to

Mode	Porous	Free-slip	Rigid
2	0.707	0.698	0.695
	1.125	1.170	1.185
3	0.577	0.559	0.553
	1.333	1.467	1.508
4	0.500	0.475	0.468
	1.563	1.810	1.887
5	0.447	0.418	0.410
	1.800	2.184	2.300
6	0.408	0.375	0.367
	2.042	2.581	2.738

TABLE 1. The degenerate points on the neutral curve, see (3.1)

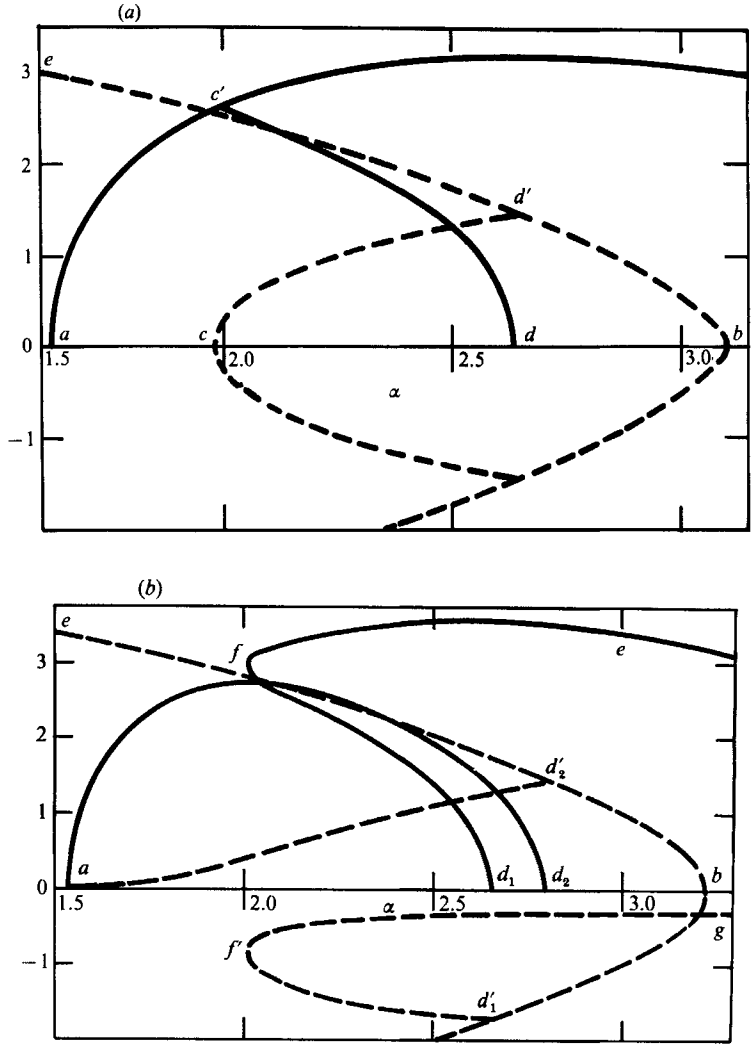

FIGURE 1(a,b). For caption see facing page.

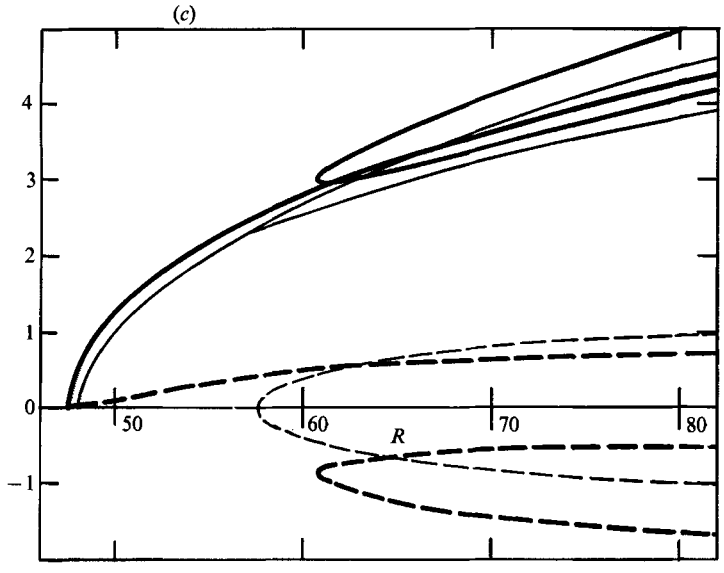

FIGURE 1. Bifurcation diagram for the modal coefficients showing the bimodal interaction of wavenumbers α and 2α for $R = 60$ and (*a*) $\beta = 0$, (*b*) $\beta = 1.0$. (*c*) The coefficients in (*a*) and (*b*) are shown as functions of R with $\alpha = 2.0$.

a new class of mixed modes which is often overlooked. Since Segel (1962) studied some of these mixed modes, such solutions have gained little attention by investigators. Most of the analytical studies in the convective systems have made use of the symmetry of the layer in order to simplify the mathematics. Thus the mixed-mode solutions are often forced out of the numerical scheme. However, once the symmetry of the layer is broken by a certain means, for example, in our case, by the temperature-dependent viscosity, the mixed modes become indistinguishable from the primary mode on the basis of the symmetry properties. One of these 'mixed modes' could eventually interchange role with the primary mode and becomes the preferred solution, if the asymmetries introduced are sufficiently strong. Thus it becomes important to identify the mixed modes and understand their bifurcation properties. The general stability dependence of these mixed modes on the viscosity gradient is of interest by itself. However, owing to our restricted stability analysis, this aspect is beyond the scope of the present study.

It is shown in Busse & Or (1986) that the bimodal interaction can exist for a pair of non-commensurate α-values. Of more physical interest, however, is that the two interacting wavenumbers are integrally related. In the (α, R)-plane, the sequence of degenerate points on the neutral curve, $(\alpha_j, R_j), j \geqslant 2$, are determined by

$$R_j = R(\alpha_j) = R(j\alpha_j). \tag{3.1}$$

the bimodal interaction between the two modes with wavenumbers α_j and $j\alpha_j$ occurs above the degenerate point (α_j, R_j). Table 1 shows a comparison of these points on the neutral curve for three convective systems: a fluid-saturated porous medium, an ordinary fluid with the free-slip boundary conditions, and with the rigid boundary condition. For the jth mode, the upper and lower figures correspond respectively to α_j/α_c and R_j/R_c. We notice that for a given j, the point in the case of the porous medium corresponds to the smallest R_j/R_c and the largest α_j/α_c ratio. The two cases corresponding to $j = 2, 3$ are of particular interest. Their domain of existence occurs

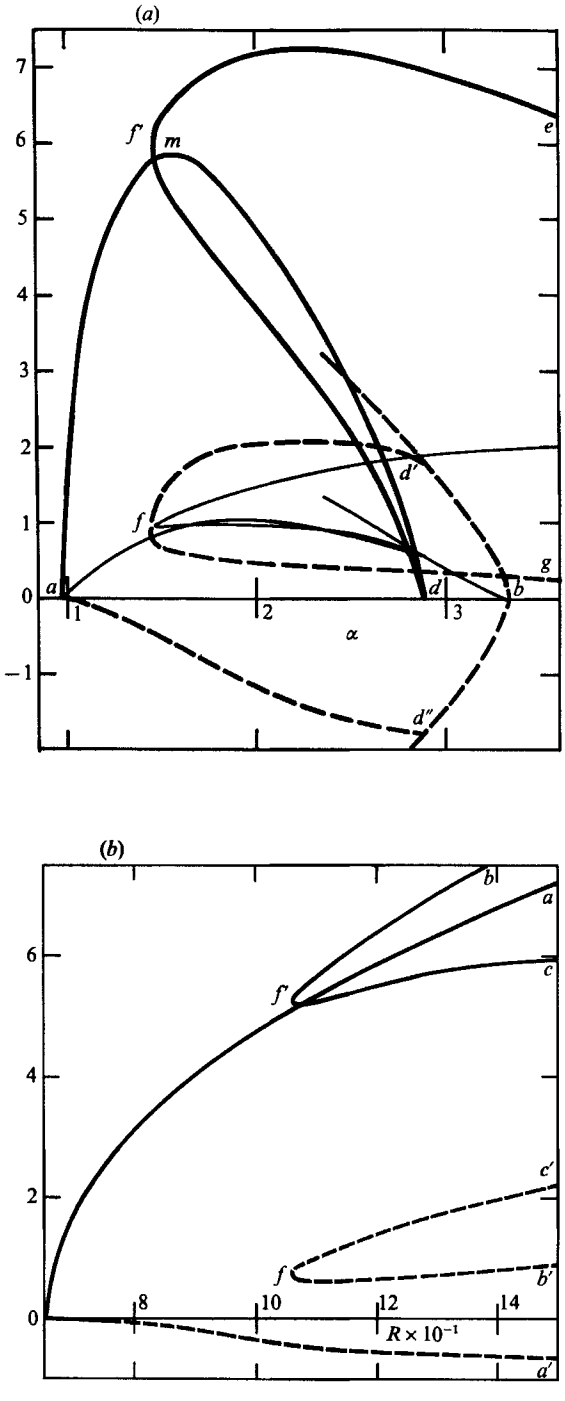

FIGURE 2. (*a*) Bifurcation diagram for the model coefficients showing the bimodal interaction of wavenumbers α and 3α for $R = 120$ and $\beta = 0$. (*b*) The coefficients in (*a*) are shown as functions of R with $\alpha = 1.5$.

closer to the critical onset and extends to overlap the stable band of the primary mode. The bifurcation structure of these two cases will be described below. The bifurcation curves are computed numerically with a truncation number $NT = 8$. In any case the Nusselt number for $NT = 8$ and $NT = 10$ differed by less than 2%.

The bimodal interaction for the α and the 2α modes is shown in figure 1. The solid and dashed curves correspond to the leading vorticity coefficients A_{11} and A_{21} respectively. Figure 1 (*a*) shows the case for $\beta = 0$ and $R = 1.52R_c$. The band width between the points *a* and *d* tends to zero at $R = 1.125R_C$. Without loss of generality, $A_{11} > 0$ is assumed, which represents a downflow at $x = 0$. The case $A_{11} < 0$ represents the same physical solution shifted by a distance of $\pi\alpha$ in x-direction. The amplitude of the primary mode is represented by the curves *ac'e* and *bd'e*. Note that the curve *bd'e* is the continuation of the curve *ac'e* over the right band where $\alpha > \pi$. This representation becomes apparent if we notice that (2.6*b*) can be rewritten as

$$\psi = \sum_{l,n}^{\infty} A_{2l,n} \sin 2l(\tfrac{1}{2}\alpha)\, x \sin \pi(z-\tfrac{1}{2}). \tag{3.2}$$

The domain of existence of the mixed mode is bounded by the harmonic and the subharmonic bifurcation points *c'* and *d'* respectively. At these points the pitchfork curves *cd'* and *dc'* emerge from the primary curve. In the literature, the dotted curves are normally represented in an orthogonal plane to the paper. Here A_{11} and A_{21} are represented on the same plane for convenience. Obviously, the mixed modes do not possess the symmetry property that corresponds to the vanishing $l+n$ coefficients in the basic solutions. From (2.6*b*), it can be shown that, assuming $A_{11} > 0$, the two cases $A_{21} > 0$ and $A_{21} < 0$ correspond respectively to fast downflow, slow upflow and vice versa. It is of interest to notice that one of these two patterns is compatible with the basic pattern modified by the presence of the vorticity gradient.

Figure 1 (*b*) shows the case for $\beta = 1$. No symmetry corresponding to even or odd $l+n$ is present anymore. Physically, the temperature-dependent viscosity is known to enhance the hot upflow jet and weaken the cold downflow jet. Thus the primary solution for $A_{11} > 0$ is associated with $A_{21} < 0$. The latter coefficient appears as the nearly horizontal dashed curve *gf'* below the α-axis. The dashed curves $ad_2', gf'd_1'$ resemble an imperfect pitchfork bifurcation that is typical from the classical theory. Compared with figure 1 (*a*), it is of interest to notice the disappearance of the harmonic bifurcation point *c* and the appearance of the turning point *f*. The subharmonic point *d* is split into two distinct points, d_1 and d_2. This splitting is necessary since the layer is no longer symmetrical with respect to the midplane. In view of this asymmetry the two subharmonic eigenmodes cannot be physically identical.

Figure 1 (*c*) shows the bifurcation diagram for $\alpha = 2.0$ and R as the abscissa. The heavy and thin curves represent the cases $\beta = 1$ and $\beta = 0$ respectively. The bimodal interaction for the α and 3α modes is shown in figure 2. Of particular interest is the case $\beta = 0$. Unlike the previous case, now both the mixed modes and the primary mode have vanishing odd $l+n$ coefficients, and thus they cannot be distinguished based on the symmetry properties alone. This non-uniqueness of solutions with the symmetry preserved occurs for $R > R_3$. In figure 2, the heavy solid and dashed curves represent A_{11} and A_{31} respectively. In figure 2 (*a*) the points *d*, *d'* and *d''* correspond to a simple degenerate subharmonic bifurcation. The horizontal band between the fold *f* and the subharmonic point *d* contains three solutions having the same symmetry properties. The primary mode is identified by the smallest A_{31}/A_{11} ratio. It is instructive to compare figure 2 (*a*) and figure 1 (*b*). The bifurcation structures for

the two cases are similar generically. In both cases, the dotted curves resemble the imperfect pitchfork. In figure 2(*a*), however, since the primary mode preserves the midplane reflection symmetry of the layer, there exists one degenerate subharmonic point instead of two distinct subharmonic points. In figure 2(*a*), the thin solid curves represent $Nu-1$, where Nu is the Nusselt number. The primary mode has the largest Nu among the three. Figure 2(*b*) shows the bifurcation curves of A_{11} and A_{31} versus R, for $\alpha = 1.5$. The similarity between figure 2(*b*) and figure 1(*c*) is also apparent.

4. The oscillatory instabilities

The oscillatory motion in porous rolls has been fairly well documented. Combarnous & Le Fur observed the two-dimensional oscillatory modes experimentally using a Hele–Shaw cell. Moore & Weiss (1973) suggested that these oscillations are caused by a resonance mechanism, which they referred to as the 'cyclic-triggering'. In effect the disturbances are generated by the periodic boost they receive from their predecessors that have circulated around the convection rolls. Horne & O'Sullivan (1974) studied porous convection rolls numerically and have provided a comparison of their result with the earlier experiment. Horne & O'Sullivan (1978) further modified the problem so that the upper boundary condition is kept at a constant pressure, thus the flow is unconfined. This arrangement minimizes the fluctuating pressure required for producing the triggering. Horne and coworkers observed similar oscillatory behaviour in the modified apparatus and thus argued that the oscillatory modes cannot be caused by the cyclic triggering. The studies by Horne & O'Sullivan appeared to favour the theory proposed by Foster (1971), who suggested that the oscillatory instabilities are caused by the thermal-boundary-layer breakdown.

Much emphasis has also been put on the accurate numerical determination of the transition parameters in the various stability domains. The work of Schubert & Straus (1979, 1982), and Kimura *et al.* (1986) furnish a comprehensive study on the sequence of motions for a wide range of the controlling parameter. Such a sequence is typical in leading to the transition to chaos. More recently, Aidun & Steen (1987) and Steen & Aidun (1988) studied the numerical convection problem with improved resolution with a square truncation scheme. The results not only provide additional resolution on the transition parameters documented earlier, but also clarify some subtle roles played by the thermal boundary layers and the pressure gradient in the transition mechanism. The results also give some important descriptions of the oscillatory mechanism.

In this section, we examine the oscillatory mode from a different perspective. We consider the instability class that has the same phase as the translational neutral disturbance of the basic state, rather than the in-phase instability class previously considered. Our result is important in indicating whether such phase dependence is important in the transition mechanism. Since α is a prescribed parameter in our infinite-periodic rolls, our result also includes the varying of α from its critical value π. On the other hand, our numerical formulation does not enable us to work in the high-resolution regime. Our truncation number NT is limited to 10. Besides determining the transition parameter for the instabilities, our emphasis is also on a simple truncated model which only retains the leading coefficients. The model gives the oscillatory instabilities via a Hopf bifurcation. The result provides some physical insight into the transition mechanism that is otherwise difficult to obtain. It is warned, however, that any comparison between our result and the exact result has

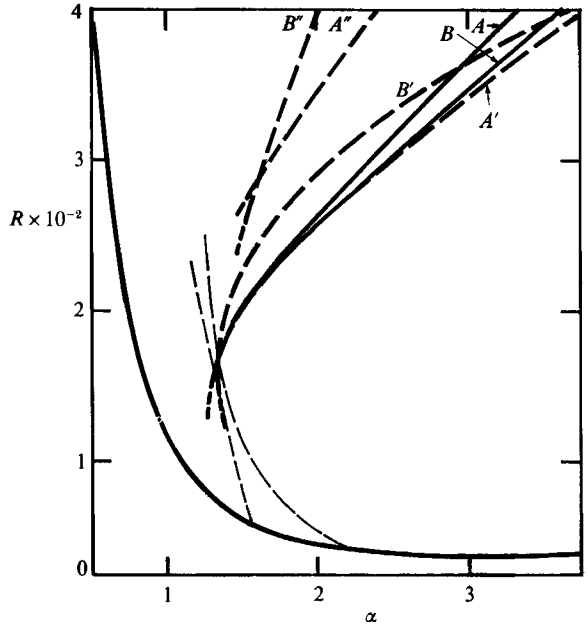

FIGURE 3. The stability diagram showing the stability boundaries of the two oscillatory instabilities (heavy lines) and the mixed-mode instabilities (thin lines) for $\beta = 0$.

to be exercised with caution, since the model suggests qualitative, rather than quantitative features.

For $\beta = 0$, figure 3 shows the stability boundaries for the first two oscillatory eigenmodes. A third unstable mode has not been observed in the proximity of the stability diagram. Both the disturbances and the basic state are at the same wavenumber. The solid curves A and B are computed with $NT = 10$ and the dashed curves A' and B', A'' and B'' are computed with $NT = 8$ and $NT = 6$ respectively. For $NT < 6$ no growing oscillatory mode can be found. Despite the large discrepancy between the cases $NT = 8$ and $NT = 6$, agreement between the cases $NT = 8$ and $NT = 10$ is much better. Since the basic state has vanishing odd $l+n$ coefficients, the disturbance eigenmodes separate into two distinct even $l+n$ and odd $l+n$ classes. We refer to them as the even and the odd mode. Both modes are oscillatory. The even and the odd mode's stability boundaries are denoted by curves A and B respectively. For the lower NT, the odd mode's boundary occurs at higher R than the even mode's. This is because we have used an even NT in truncating the basic and the disturbance solutions in the computation, thus the odd mode suffers a more severe truncation error. For $\alpha = \pi$ and $NT = 10$, the condition $\mathrm{Re}\,\sigma = 0$ for the even and the odd oscillatory mode occurs at $R = 383$ and 359 respectively, where the corresponding values for $\mathrm{Im}\,\sigma$ are respectively 528 and 443. For comparison, the corresponding exact values for the onset of the in-phase oscillatory mode reported by Aidun & Steen (1987) are $R = 391$ and $\mathrm{Im}\,\sigma = 521$. In figure 3, the stability boundaries cannot be computed for α less than a value somewhere between 1.3 and 1.4 where, as indicated from figure 2(*a*), a turning point f occurs in the basic state. To see if the oscillatory instabilities exist to the left of the fold f, we perturb the basic state from the left branch of the neutral curve. In this case no unstable oscillatory eigenmodes are found. As we increase R, a steady unstable eigenmode first occurs when R exceeds R_2.

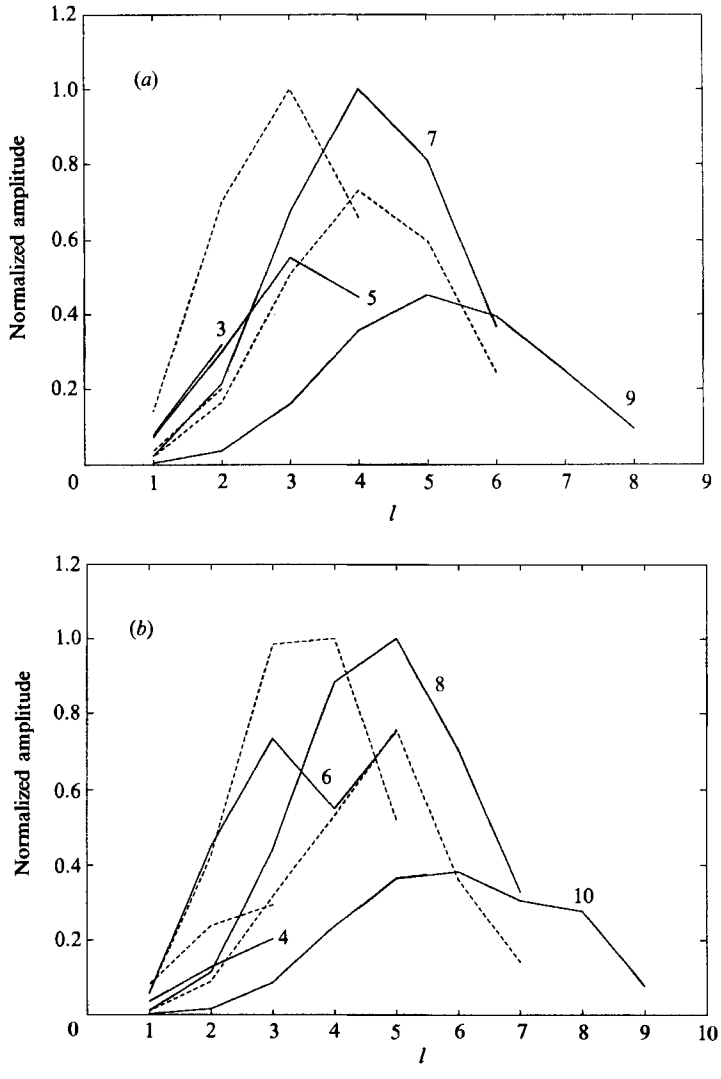

FIGURE 4. (*a*) The distribution of the normalized amplitude coefficients of the Fourier modes of (*a*) the odd and (*b*) oscillatory modes of instability with respect to L and l.

A second steady unstable eigenmode occurs when R exceeds R_4, and so on. As α increases away from the neutral-curve value, σ decreases and passes through zero where the pitchfork bifurcation to the mixed modes occurs. The loci for these bifurcation points correspond to the stability boundaries shown as the thin dashed lines in figure 3.

The amplitude-coefficient distribution of the oscillatory instability eigenvectors is substantially different from that of the basic state. To see this, we plot the scaled magnitude of the Fourier coefficients of the vorticity, $|\tilde{A}_{ln}|$, of the two unstable eigenmodes. Figures 4(*a*) and 4(*b*) show respectively the odd and even unstable oscillatory modal distributions. The dotted and solid lines represent the cases NT = 8 and 10 respectively. Each line is associated with an integer L whose value is marked along each solid line, and connects the Fourier modes such that the sum of the indices

$l+n=L$. The abscissa is the index l. It is observed that dominant Fourier modes have $L=NT-2$ in the even mode and $L=NT-3$ in the odd mode. For the larger NT (the solid lines), the Fourier modes connected by the lines with $L=NT$ (even mode) and $L=NT-1$ (odd mode) are more evenly distributed, while the Fourier modes connected by the lines with $L=NT-2$ (even mode) and $L=NT-3$ (odd mode) possess sharper peaks. For the odd mode, figure 4(*a*) shows that $|\tilde{A}_{45}|$ and $|\tilde{A}_{54}|$ dominate. For the even mode, figure 4(*b*) shows that $|\tilde{A}_{46}|$ and $|\tilde{A}_{55}|$ dominate. The contrast is expected to be even more pronounced when the energy, or the square of the amplitude, is plotted instead. In our truncated model, only the modes connected by the line possessing the peak are considered. Steen & Aidun (1988) have also tabulated the leading coefficients of the unstable eigenmode (see their table 2). In their distribution, the same trend has been observed. However, since the representative functions used in their expansions are somewhat different from the ones used here, the dominant coefficients cannot be compared directly. In contrast to the unstable eigenmodes, the distribution of the leading coefficients of the basic state where the eignmodes are derived is substantially different. The leading coefficients in the basic state in descending magnitude are: $A_{11}=16.2, A_{31}=2.49$, $A_{22}=1.7, A_{13}=1.1$. Other coefficients are considerably smaller. It is clear that the steady state has its energy concentrated in the lowest few modes. It is very likely that the oscillatory instability is to provide a means of transferring the energy to the smaller scales.

In the following, we construct a truncated model which can allow us to gain some insight into the mechanism. The model has a basic state which consists of the fundamental mode A_{11} and the mean temperature distortion coefficients, B_{0k}, for even k. The scheme is not a small-amplitude expansion about the critical onset. The values of the coefficients used in the model are obtained from the exact numerical solution. The basic state is perturbed by the disturbances consisting of the Fourier modes whose coefficients satisfy $l+n=L$. We essentially drop coefficients of secondary importance to the oscillatory mechanism, and force a low-dimensional eigenvalue problem that approximates the original one. The truncated heat equation in our model becomes

$$H_{ij}\tilde{B}_{L-i,j}=0, \quad i,j=1,2,\ldots L-1, \tag{4.1a}$$

where

$$H_{kk}=\sigma+a^2_{L-k,k}+(L-k)\,\alpha r_{L-k}(-1-k\pi B_{0,2k})$$

and

$$H_{k,k+1}=-\tfrac{1}{4}\pi\alpha L\left(1+\frac{r_{L-k-1,k+1}}{r_{11}}\right)A,$$

$$H_{k+1,k}=\tfrac{1}{4}\pi\alpha L\left(1-\frac{r_{L-k,k}}{r_{11}}\right)A,$$

where k varies from 1 to $L-1$ for H_{kk} and from 1 to $L-2$ for the subdiagonal elements. All other matrix elements of H_{ij} vanish. In obtaining (4.1*a*) the linear vorticity equation

$$\tilde{A}_{ln}=-r_{ln}\tilde{B}_{ln} \tag{4.1b}$$

has been used, where $A=A_{11}, a^2_{ln}=(n^2\pi^2+l^2\alpha^2)$, and $R=\chi R_0$. The porous and the ordinary convection rolls are different in the values of R_0, α_c and r_{ln}. For the porous rolls, we have

$$R_0=\frac{a^4_{11}}{\alpha^2}, \quad r_{ln}=\frac{l\alpha R}{a^2_{ln}}, \quad \alpha_c=\pi, \quad R_c=4\pi^2, \quad \text{thus } r_{ln}=\frac{4l\pi\chi}{n^2+l^2} \quad \text{at} \quad \alpha=\alpha_c.$$

For ordinary convection rolls, we have

$$R_0 = \frac{a_{11}^6}{\alpha^2}, \quad r_{ln} = \frac{l\alpha R}{a_{ln}^4}, \quad \alpha_c = \pi/\sqrt{2}, \quad R_c = \tfrac{27}{4}\pi^4,$$

$$\text{thus } r_{ln} = \frac{27l\pi\chi}{\sqrt{2}(2n^2+l^2)^2} \quad \text{at} \quad \alpha = \alpha_c.$$

The diagonal elements H_{kk} correspond to the linear terms in the heat equation with a modified mean temperature profile. The subdiagonal elements represent the leading nonlinear effect of the temperature advection. In this model, the growth rate, $\mathrm{Re}\,\sigma$, depends only on the diagonal elements. The term $a_{L-k+1,k}^2$ in H_{kk} represents the thermal diffusion effect that tends to smooth out the disturbance. This effect is counteracted by the vertical advection of the disturbance temperature along the modified thermal gradient. It is observed from the steady-state solutions that all the mean coefficients $B_{0,2k}$ have the same sign. Thus the gradient in the interior of the layer is flat while the gradient near the boundaries is steep. Noticeably, the value of the coefficient B_{02} becomes saturated near $1/\pi$ for large R. Notice that $|B_{02}|$ cannot increase indefinitely since the modified gradient is not expected to locally reverse sign. From (4.1*a*) we observe that in the regime where the oscillatory modes are excited (about 10–15 times above the critical onset), the coefficients B_{0k} are only effective in stablizing the single-roll disturbance ($n = 1$). The multi-roll disturbances ($n \geqslant 2$) can be excited by the static temperature gradient since $B_{0k} \ll B_{02}$ *for* $k \geqslant 4$, which implies that the stabilizing effect due to the mean-profile distortion from these disturbances is relatively weak. With the truncated model, we show that the oscillatory instabilities are instabilities caused by the effect of the static thermal gradient. For the porous rolls, this effect operates in the range of R where the transition has been observed. But for the ordinary convection rolls, this effect corresponds to much higher R. This effect is obviously consistent with the idea that the thermal-boundary-layer breakdown triggers the oscillatory mtions. It should be remarked that the asymptotic theory of an unstable thermal boundary layer yields a much higher R than the range addressed here (see Busse 1978). In fact, in ordinary convection, Krishnamurti (1970) observed experimentally that the oscillatory behaviour operates at considerable lower R than that given by the asymptotic expression. In order to explain why the transition to the multi-roll instability takes the oscillatory route, we observe that there exists a restoring mechanism as seen through the signs of the subdiagonal elements of H_{ij}. Coupling by the basic rolls, the disturbance Fourier modes operate as a pair. As soon as one dominant mode grows, it also transfers energy to the other mode. As it decays, the other mode transfers energy back to it.

To illustrate the model, let us consider the case $L = 7$ and $L = 8$, where the interaction is between the pair of most dominant Fourier modes. From figure 4 such a pair of modes is in the form of $\tilde{B}_{L-j,j}$ and $\tilde{B}_{L-j-1,j+1}$, where $j = 2$ for $L = 7$ and $j = 3$ for $L = 8$ respectively. From the steady state for $R = 400$, $\alpha = \pi$ and $NT = 10$, we have $A = 16.2$, $B_{02} = -0.34$, $B_{04} = -0.088$, $B_{06} = -0.026$, $B_{08} = -0.0077$, and $B_{010} = -0.0030$. These values are not sensitive to R in the proximity of the stability boundary, and are used in (4.1). The following quadratic equation in σ is obtained:

$$\sigma^2 + Q\sigma + S = 0, \tag{4.2}$$

where

$$Q = a^2_{L-j,j} + a^2_{L-j-1,j+1} + (L-j)\,\alpha r_{L-j,j}(-1-j\pi B_{0,2j}) + (L-j-1)\,\alpha r_{L-j-1,j+1}(-1-(j+1)\,\pi B_{0,2(j+1)}),$$

$$S = [a^2_{L-j,j} + (L-j)\,\alpha r_{L-j,j}(-1-j\pi B_{0,2j})]\,[a^2_{L-j-1,j+1} + (L-j-1)\,\alpha r_{L-j-1,j+1}(-1-(j+1)\,\pi B_{0,2(j+1)})] + \tfrac{1}{16}(L\pi\alpha)^2\left(1-\frac{r_{L-j,j}}{r_{11}}\right)\left(1+\frac{r_{L-j-1,j+1}}{r_{11}}\right)A^2.$$

Substituting the steady-state values into the above equation, we observe that $S > 0$ and the term involving the amplitude A is about an order of magnitude larger than the first product term. The neutral stability, $\mathrm{Re}\,\sigma = 0$, is determined from

$$Q = 0. \tag{4.3}$$

The last condition enables us to determine χ_c, the critical onset ratio R/R_c at the stability boundary. In turn, $\mathrm{Im}\,\sigma$ can be determined by substituting χ_c into the expression for S. The results we obtain are: (i) $\chi_c = 15.5$, $|\mathrm{Im}\,\sigma| = 255$ for the odd mode, where $L = 7$; and (ii) $\chi_c = 16.3$, $|\mathrm{Im}\,\sigma| = 300.1$ for the even mode, where $L = 8$. The onset values of R and frequency of the oscillation in this simple model are respectively factors of approximately 1.5 and 1.75 of the exact values. Apart from the shift in values, however, the simple model predicts the trend and the interaction mechanism. It is of interest to observe that the χ_c for the odd mode is much closer to the exact value if the stabilizing effect of the mean gradient distortion is completely ignored. In this case we have χ_c equal to 9.0, or $R = 359.2$. Correspondingly, the χ_c for the even mode is about 13.3, which is still considerably higher than the exact value.

The question remains why the oscillatory modes are not observed in the ordinary convection rolls. Consider the condition (4.3) for the ordinary rolls. Ignore the stabilizing mean-gradient distortion effect. The condition, which we shall not go into in detail, gives a χ_c at least 3 times as high as the porous rolls. Since R_c of the ordinary rolls is about 16 times that of the porous rolls, we thus expect an R onset value of oscillatory motion at least on the order of 10^4–10^5. Such value of R is seldom reachable through a modestly truncated numerical scheme.

More insight can also be gained by studying the neutral curves at α_c. The R/R_c-value at $\alpha = \alpha_c$ is given by

$$\left.\begin{aligned} &\frac{(n^2+l^2)^2}{4l^2} && \text{for the porous rolls,}\\ &\frac{(2n^2+l^2)^3}{27l^2} && \text{for the ordinary rolls,}\end{aligned}\right\} \tag{4.4}$$

where n, l are the indices of z and x respectively. The lowest few modes for each case are plotted in figure 5. The solid lines connect the porous modes and the dotted lines connect the ordinary modes. Each ascending line corresponds to an increasing integer of n that starts from $n = 1$. The abscissa represents the index l. Except for $n = 1$, every line exhibits a minimum at a certain l. The lines for the porous rolls are relatively flat for larger l; while the lines for the ordinary rolls are much steeper for larger l. The ordinate value for the ordinary rolls increases rapidly between $n = 2$ and $n = 3$ and thereafter; while such value appears to increase much slower with n for the

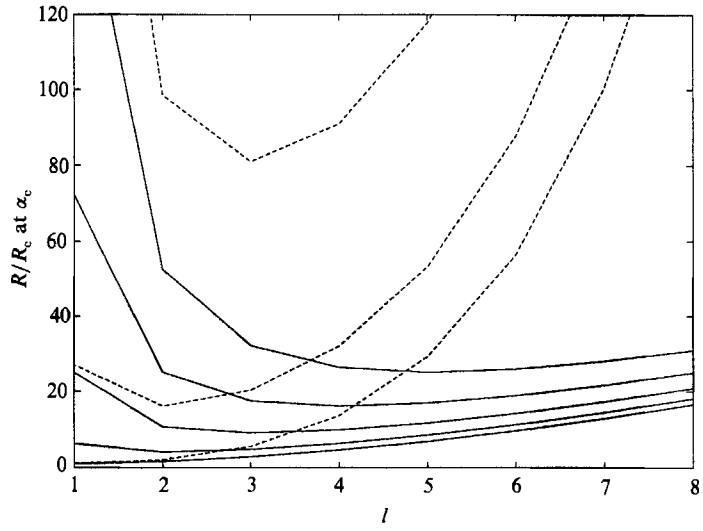

FIGURE 5. The R/R_c ratio of the family of neutral curves at α_c for various n as functions of l. The solid and dotted lines connect respectively the modes of the porous and ordinary convection rolls.

β	σ (odd mode)	σ (even mode)
0	(−6.16, 299.52)	(3.46, 376.54)
0.5	(−15.62, 316.40)	(14.75, 364.26)
1.0	(−59.36, 353.20)	(71.37, 361.43)

TABLE 2. The variation of σ for the even- and odd-mode oscillatory instabilities with β (Note: Im σ has both signs)

porous rolls. From figure 5, it is apparent why the oscillatory modes occur in the lower-order porous system but not the ordinary convection system.

To see how the growth rate and frequency of the oscillatory modes are affected by β, we compute σ as a function of β. The steady state is perturbed at $R = 360$, $\alpha = \pi$, and $NT = 8$. Table 2 shows that the odd mode is stabilized while the even mode is destabilized as β increases.

5. The non-oscillatory instabilities of the mixed solutions

For $\beta = 0$, the oscillatory and the Eckhaus modes are the only two-dimensional instabilities that the primary steady-state solutions exhibit. The Eckhaus mode requires a wavenumber modulation and has not been captured here. We have followed the eigenmodes to see if any such mode could be destabilized by a non-vanishing β. From our formulation, it is observed that such a case will give the mean-flow instability. Unfortunately, our result does not show such a mode for R as high as 25 times above the critical onset.

To look for a possible mean-flow-generating instability, the remaining possibility lies in perturbing the mixed modes. For $\beta = 0$, each of these modes is associated with a growing non-oscillatory eigenmode of disturbance. There is no mean-flow term generated for $\beta = 0$ since the vorticity equation is linear. In this case the instability appears trivially, to shift the mixed mode back to the primary mode. However, when

solution	β	A_{11}	A_{21}	Nu	σ
I	0	1.05	1.39	1.35	(0.169, 0)
	1.0	1.74	1.16	1.49	(3.54, 0)
II	0	1.049	−1.39	1.35	(0.169, 0)
	1.0	1.10	−1.69	1.48	(−1.197, 0)

TABLE 3. Showing the dependence of the major coefficients, Nu, and σ of the two mirror-symmetric mixed modes on β

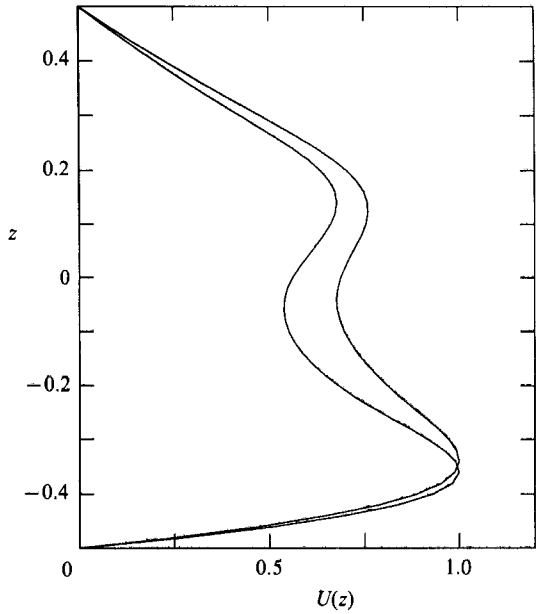

FIGURE 6. The normalized disturbance mean-flow profiles generates by the instabilities of the two mixed modes corresponding to the α and 2α bimodal interaction.

$\beta \neq 0$, the mixed mode becomes unstable to a $\frac{1}{2}\pi$ phase-shifted disturbance that carries a mean component of $O(\beta)$. Owing to this mean component, the instability cannot just shift the mixed mode back to the primary mode. It thus suggests the presence of a new steady-state equilibrium that possesses a mean shear.

As an actual example, the instability on the mixed modes resulting from the bimodal interaction of wavenumbers α and 2α is shown in table 3. In this case we have $R = 60$ and $\alpha = 2.55$. At $\beta = 0$, the two modes ($A_{11}, A_{21} < 0$ and $A_{21} > 0$) have the same σ. Notice that $\mathrm{Im}\,\sigma = 0$. At $\beta = 1$, the mode with $A_{21} > 0$ is destabilized while the other mode is stabilized. It is of interest to show the mean velocity of the unstable eigenmodes of these two mixed modes. Figure 6 show the normalized velocity. The two profiles are very similar. The velocity is stronger towards the lower half of the layer where the fluid is less viscous. The profile with slightly weaker velocity corresponds to the mixed mode with $A_{21} < 0$.

6. Discussion and concluding remarks

The existence of a hierarchy of oscillatory instabilities in the convection rolls of a fluid-saturated porous medium offers an excellent opportunity for the study of the transition to chaos in actual fluid systems. Considerable progress has been demonstrated by the work of Kimura *et al.* (1986). The route to chaos through preserving the two-dimensionality is particularly attractive to numerical analysts since it requires relatively small computational resources. Examples that offer such an attractive feature are quite rare in real fluid systems. However, it is worth remarking that there are other means to preserve the two-dimensionality, apart from using the large-aspect-ratio geometry in the Hele–Shaw apparatus. In a thermal Rossby wave, the two-dimensionality is constrained instead by the rapid rotation. Or & Busse (1987) also observe numerically the transition to chaos through a period-doubling sequence. The transition does not have the symmetry properties of the Hopf bifurcations since the frequency is non-vanishing in the basic state of the wave.

In in-phase oscillatory instabilities investigated by previous authors and the phase-shifted oscillatory instabilities in the infinite extent investigated here are physically distinct. It is thus natural to expect a difference in the transition parameters. The comparison of the parameters with previous work in §4, however, shows that this difference is quite small in R. It appears reasonable to infer that the in-phase modes and the phase-shifted modes are operated by a similar mechanism. Furthermore, in our case, the distinction between the odd mode ($L = 7$) and the even mode ($L = 8$) appears to be caused by the symmetry introduced by the flow-field representation functions, since the two modes are so close that it would be reasonable to expect that their difference diminishes if the symmetry in the basic rolls is removed. This view seems consistent with the result that an increase of β draws the stability boundaries closer together.

The existence of the finite-amplitude solution which carries a mean velocity of $O(\beta)$ is of interest for future work. Such a solution and its stability is of geophysical significance. The problem, however, requires a more general formulation of both the steady-state solver and the stability analysis that can relax the reflection symmetry of the rolls. It could be an interesting area of study for further work.

The author wants to thank Professor F. H. Busse, who formulated the original problem and provided many helpful discussions for this problem. I am also indebted to Professor P. S. Marcus, who provided many helpful discussions and supported this work through a grant from National Science Foundation (AST-8796285), and a grant from Lawrence Livermore Laboratory. The computation was mainly done in the Center for Astrophysics, Harvard University.

REFERENCES

Aidun, C. K. & Steen, P. H. 1987 Transition to oscillatory convective heat transfer in a fluid-saturated porous medium. *J. Thermophys.* **1**, 268–273.

Busse, F. H. 1967 On the stability of two-dimensional convection in a layer heated from below. *J. Maths & Phys.* **46**, 140–150.

Busse, F. H. 1983 Generation of mean flows by thermal convection. *Physica* **9D**, 287–299.

Busse, F. H. & Clever, R. M. 1979 Instabilities of convection rolls in a fluid of moderate Prandtl number. *J. Fluid Mech.* **91**, 319–335.

Busse, F. H. & Or, A. C. 1986 Subharmonic and asymmetric convection rolls. *Z. Angew. Math. Phys.* **37**, 608–623.

COMBARNOUS, M. & LE FUR, B. 1969 Transfert de chaleur par convection naturolle dans une couche poreuse horizontale. *C.R. Acad. Sci. Paris* **269B**, 1009.

FOSTER, T. D. 1971 Intermittent convection. *Geophys. Fluid Dyn.* **2**, 201–217.

HAGER, B. H. & O'CONNELL, R. J. 1981 A simple global model of plate dynamics and mantle convection. *J. Geophys. Res.* **86**, 4843–4867.

HORNE, R. N. & O'SULLIVAN, M. J. 1974 Oscillatory convection in a porous medium heated from below. *J. Fluid Mech.* **66**, 339–352.

HORNE, R. N. & O'SULLIVAN, M. J. 1978 Origin of oscillatory convection in porous medium heated from below. *Phys. Fluids* **21**, 1260–1264.

KIMURA, S., SCHUBERT, G. & STRAUS, J. M. 1986 Route to chaos in porous medium thermal convection. *J. Fluid Mech.* **166**, 305–324.

KRISHNAMURTI, R. 1970 On the transition to turbulent convection. Part 2. The transition to time-dependent flow. *J. Fluid Mech.* **42**, 309–320.

MOORE, D. R. & WEISS, N. O. 1973 Two-dimensional Rayleigh–Bénard convection. *J. Fluid Mech.* **58**, 289–312.

OR, A. C. & BUSSE, F. H. 1987 Convection in a rotating cylindrical annulus. Part 2. Transition to asymmetric and vascillating flow. *J. Fluid Mech.* **174**, 313–326.

SAFFMAN, P. G. & TAYLOR, G. I. 1958 The penetration of a fluid into a porous medium or Hele–Shaw cell containing a more viscous liquid. *Proc. R. Soc. Lond.* A **245**, 312–329.

SCHUBERT, G. & STRAUS, J. M. 1979 Three-dimensional and multicellular steady and unsteady convection in fluid-saturated porous media at high Rayleigh numbers. *J. Fluid Mech.* **94**, 25–38.

SCHUBERT, G. & STRAUS, J. M. 1982 Transitions in time-dependent thermal convection in fluid-saturated porous media. *J. Fluid Mech.* **121**, 301–313.

SEGEL, L. A. 1962 The nonlinear interaction of two disturbances in the thermal convection problem. *J. Fluid Mech.* **14**, 97–114.

STEEN, P. H. & AIDUN, C. K. 1988 Time-periodic convection in porous media: Transition mechanism. *J. Fluid Mech.* **196**, 263–291.

STRAUS, J. M. 1974 Large amplitude convection in porous media. *J. Fluid Mech.* **64**, 51.

STRAUS, J. M. & SCHUBERT, G. 1979 Three-dimensional convection in a cubic box of fluid-saturated porous material. *J. Fluid Mech.* **91**, 155–165.